Urol Res (2004) 32: 28–35
DOI 10.1007/s00240-003-0370-x

ORIGINAL PAPER

M. Abend · M. Port · H. U. Schmelz · K. Kraft
C. Sparwasser

Significance of apoptosis in metastasizing testis tumors

Received: 7 May 2003 / Accepted: 8 September 2003 / Published online: 25 October 2003

Abstract Testis tumors of embryonal origin (ten metastasized, six non-metastasized) and 17 mixed testis cell carcinomas (eight metastasized, nine non-metastasized) were examined. A triple immunofluorescence microscopic labeling procedure allowed the simultaneous detection of two features of apoptosis, namely morphological changes in the nucleus (DNA condensation visualized by DAPI staining) and the process of DNA fragmentation (TdT-assay) in tumor cells as well as T-cells (recognized by their CD45RO epitope). Both methods for apoptosis detection showed similar apoptotic indices (AI) only in 2.6% of all tumors. Most tumors (81.6%) showed more cells with DNA fragments than condensed chromatin, but in a number of cases (10.5%) the opposite pattern was found. These data add to the few published in vivo examinations of apoptosis using different methods and help to explain differences in the judgment of apoptosis significance for tumor prognosis. With regard to tumorigenesis, non-metastasized testis tumors were characterized by higher AIs of tumor cells and T-cells compared with metastasized tumors, which could be interpreted as a characteristic of tumors in an earlier stage of their development into an apoptosis-resistant phenotype. For the first time, in metastasized tumors a 5 to 25-fold increase of the T-cell's AIs over the corresponding AIs of tumor cells was shown. This suggests a successful counterattack of tumor cells, thus supporting the process of metastasis. However, only ten out of 33 tumors revealed these AI changes, which again highlights that tumor biology cannot be predicted by a single parametric approach. It remains to be seen whether these characteristics might be suitable for a reliable prediction of metastasis.

Keywords Apoptosis · Metastasis · Testis tumors · Tumor infiltrating lymphocytes · Immunofluorescence microscopy

H. U. Schmelz (✉) · C. Sparwasser
Department of Urology, Federal Armed Forces Hospital,
Oberer Eselsberg 40, 89081 Ulm, Germany
E-mail: hansulrichschmelz@bundeswehr.org
Tel.: +49-731-17102101
Fax: +49-731-17102108

M. Abend · M. Port
Institute of Radiobiology,
Federal Armed Forces, Munich, Germany

K. Kraft
Department of Pathology,
Federal Armed Forces Hospital, Ulm, Germany

Introduction

Malignant neoplasms are known to be composed of diverse cell populations that are heterogeneous in respect to a variety of properties, including the ability to metastasize. In this context, the question arises as to whether there is a metastatic phenotype and, if so, what its cellular properties are.

Apoptosis has been widely used for diagnosis and prognosis of cancer [13, 20, 26, 31]. However, different reports have come to contrary conclusions concerning the significance of apoptosis in tumorigenesis [2, 9, 16, 24, 27]. One explanation is that short-term assays (e.g., dye exclusion, apoptosis measured only at a certain point in time) for cell killing were used instead of clonogenicity and that in tumors a selection in favor of the apoptotic-resistant phenotype takes place [4, 27].

Reports dealing with this question frequently fail to consider diverse cell populations. According to concepts of tumor immunology, tumor-infiltrating lymphocytes (e.g., T-cells) are believed to attack and eliminate tumor cells [12]. To reach a clinically detectable size, neoplasms must be able to suppress or evade this host immune response.

Moreover, apoptosis represents a multi-step process. In 1972, Kerr, Wyllie and Currie introduced the term *apoptosis* to describe a process of cell death characterized by certain unique morphological features (cell shrinkage, DNA condensation along the nucleus membrane, budding of the cell soma, single cell death without inflammatory reactions) [11]. With the advent of

biochemical techniques such as DNA electrophoresis in the 1980s apoptosis became linked to certain processes of DNA cleavage. In some models of apoptosis, activated intracellular endonucleases disrupt DNA at the higher chromatin order, leading to DNA fragments in the range of 50, 300, 700 and 1000 kbp [29, 30]. With the release of endonucleases which disrupt these higher chromatin fragments internucleosomally, DNA fragments of 180 bp and multiples of it can be visualized as a so-called laddering pattern on gel electrophoresis. The DNA ladder, it has been suggested, is a hallmark of apoptosis. This suggests that the multi-step process of apoptosis should be examined using several different methods simultaneously. Most publications are characterized by a lack of different methods for apoptosis detection.

In order to elucidate the significance of apoptosis for the process of metastasis, metastasized, as well as non-metastasized, testis tumors were investigated. Two major features of apoptosis, namely morphological changes taking place in the nucleus (DNA condensation of the chromatin) and the endonucleolytical cleavage of the chromatin (DNA fragmentation), were examined in tumor cells and T-cells simultaneously. This made it possible to measure the successful attack of T-cells in tumor cells and the counterattack of the tumor cells, which caused the induction of apoptosis in T-cells. Based on these measurements, different apoptotic indices (AI) were calculated for tumor cells and T-cells and correlated with clinical data such as for metastasis.

Table 1 Characteristics of the patients and their tumors

#	Age	Histology	Metastasis	TNM stage
1	38	ECC	–	pT1cN0M0
2	33	ECC	–	pT1pN0M0
3	30	ECC	–	pT1pN0M0
4	20	ECC	–	pT1cN0M0
5	21	ECC	–	pT1cN0M0
6	21	ECC	–	pT1cN0M0
7	21	ECC	+	pT1pN1M0
8	24	ECC	+	PT1pN1M0
9	21	ECC	+	pT1pN1M0
10	25	ECC	+	pT1cN1M0
11	24	ECC	+	pT1pN2M1
12	53	ECC	+	pT1cN0M1
13	32	ECC	+	pT1pN1M0
14	24	ECC	+	pT1pN2M0
15	21	ECC	+	pT1pN1M0
16	21	ECC	+	pT1cN0M1
17	19	ECC + CC	–	pT1pN0M0
18	31	Sem + ECC	–	pT2pN0M0
19	29	Sem + ECC	–	pT2pN0M0
20	25	ECC + Ter + YST	–	pT1pN0M0
21	29	ECC + CC + Ter + YST	–	pT3N0M0
22	42	ECC + YST	–	pT1pN0M0
23	27	ECC + Ter	–	pT1N0M0
24	25	Sem + ECC + Ter + YST	–	pT1pN0M0
25	29	Sem + ECC + CC + Ter	–	pT1pN0M0
26	23	ECC + YST	+	pT1pN1M0
27	22	Ter + ECC	+	pT1pN2M0
28	19	ECC + CC + YST	+	pT1pN1M0
29	22	ECC + YST	+	pT1pN1M0
30	22	ECC + YST	+	pT1pN2M0
31	25	ECC + Ter + CC	+	pT1pN2M0
32	23	ECC + Ter + YST	+	pT1pN1M0
33	24	ECC + Ter + YST	+	pT1N2M0

ECC embryonal cell carcinoma, *CC* chorion carcinoma, *Sem* seminoma, *Ter* teratoma, *YST* yolk sack tumor

Materials and methods

Tissue

Tissue samples obtained from 33 patients with 16 embryonal cell carcinoma (ten metastasized, six non-metastasized) and 17 mixed cell tumors (eight metastasized, nine non-metastasized) containing tissue of different origin (predominantly seminoma, chorion and embryonal cells) were examined (Table 1). More than 80% of the patients were between 20–30 years of age at the time of the operation. Most tumors were characterized by a T1 tumor size and a lymph node status ranging between N0 and N2 (Table 1). The cases were selected from the files of diagnosed surgical specimens of the Department of Pathology, Federal Armed Forces Hospital, Ulm, Germany. Informed consent was obtained from all patients. Tissues were fixed in 4% buffered formalin paraffine-embedded and processed by standard methods. Consecutive sections (5 μm) were mounted on coated slides (Superfrost/Plus, Menzel Gläser, Munich, Germany). One section was processed for the immunological in situ end labeling (ISEL) of DNA fragments. On the same slide, tumor-infiltrating T-cells, as well as the nuclei, were visualized using immunofluorescence microscopy. Under the guidance of an experienced pathologist, a second section was stained with hematoxyline eosin to define the tumor region.

In situ end labeling (ISEL), T-cell detection and DNA counterstain

After deparaffination and rehydration, tissue sections were heated three times in citrate buffer in a common microwave oven (Fa. Bauknecht, Schondorf, Germany) at 900W for 8 min, 620 W for 6 min and 900 W for 4 min to facilitate antigen retrieval. After washing with water (twice) and phosphate buffered saline (once), the ApopTaqPuls Kit (Oncor, Appligene, Heidelberg, Germany) was used for ISEL as published recently [1], but proteinase K digestion was replaced by the microwave procedure as described above. Finally, DNA fragments were labeled with an anti-digoxigenin FITC conjugate. The labeling of DNA fragments was combined with the detection of T-cells using a CD45RO mouse primary antibody (clone OPD4, Dako, Hamburg, Germany) which was detected with a rabbit anti-mouse Cy3 conjugated secondary antibody (Dianova, Hamburg, Germany). In order to intensify the signals, the staining of T-cells had to be repeated. The DNA-specific dye 4',6-diamidino-2-phenylindole (DAPI, final concentration was 1 μg/ml; Serva, Heidelberg, Germany) was added for examination of the nucleus apoptosis morphology and incubated for 5 min. Slides were washed three times with distilled water, dried at room temperature and mounted in glycerol/paraphenylenediamine (PPD, antifading drug; final concentration 1 mM, Aldrich, Steinheim, Germany). The details of this triple immunofluorescence staining procedure and the sequence of major steps are shown in Table 2.

HL-60 cells served as a positive control for ISEL. Irradiated HL-60 cells (irradiation increases the apoptosis frequency) were similarly treated, except that heating in the microwave oven was omitted. For negative controls, consecutive sections of the tissues examined were treated in the same way, but neither TdT enzyme nor the primary antibody for T-cell detection were added to the reaction mixtures on the slides. Optimization of the method (time and power of the microwave treatment and comparison with different regimens of proteinase K digestion) was determined in a cascade of preliminary experiments (not shown). Cells with an FITC signal in the nucleus were considered to contain fragmented DNA. Cells labeled with a red ring around the cells were considered to represent T-cells.

Table 2 Sequence of major steps for the triple immunofluorescence staining procedure of DNA fragments, condensed chromatin and T-cells

Labeling steps	Detection of:		
	DNA-fragments	DNA-condensation	T-cells
1	TdTmix containing digoxigenated nucleotids and terminal transferase	–	–
2	–	–	Primary antibody
3	–	–	Cy-3-conjugated sec. antibody
4	–	–	Primary antibody
5	Anti-digox. FITC	–	Cy-3-conjugated sec. antibody
6	–	DAPI incubation	–

Microscopic examination and definition of different apoptotic indices (AI)

The slides were scored at 400–1000× with the aid of an epifluorescence microscope (DM RB, Leica, Bensheim, Germany). A filter block for DAPI excitation (excitation: 270–380 nm; emission: 410–580 nm) enabled the detection of morphological changes in the nucleus characteristic of apoptosis (DNA condensation). When changing the filter block with the filter wheel, the same cells were examined for FITC signals (excitation: 450–490 nm; emission: 520 nm, long pass filter) enabling us to detect apoptotic cells characterized by DNA fragmentation caused by endonucleolytic DNA cleavage. A further filter change for detection of Cy-3 signals (excitation: 546–552 nm; emission 570 nm) made it possible to discriminate between T-cells and the remaining population of cells located in the tumor cell region.

With this procedure, apoptosis in two different cell populations could be quantified using two different methods for apoptosis detection. The following AIs were defined for tumor cells as well as T-cells:

1. AI representing the number of cells characterized by DNA fragmentation only, $AI_{DNAfrag}$ (detection: FITC signal only)
2. AI representing both DNA fragmentation and condensation, $AI_{frag\&cond}$ (detection: FITC signal as well as typical nucleus morphology using DAPI)
3. AI representing the number of cells characterized by DNA condensation only, $AI_{DNAcond}$ (detection: no FITC signal, but typical nucleus morphology shown with the aid of DAPI)
4. The sum of $AI_{DNAfrag}$, $AI_{DNAcond}$ and $AI_{frag\&cond}$ was considered to represent the total number of apoptotic cells ($AI_{totalapopt}$)

Statistics

In each testis tumor, 15 microscopic fields representing different regions of the tumor were scored and then the mean values were calculated. This amounts to 1750 ± 570 examined cells. Descriptive statistics was compiled using Sigma Plot 2000 (Jandel, Erkrath, Germany). Significant levels were calculated with the t-test employing Sigma Stat (Jandel, Erkrath, Germany). P values < 0.05 were considered to reflect a statically significant difference.

Results

Comparison of $AI_{DNAfrag}$ with $AI_{DNAcond}$ independent of cell type and tumor entity

When comparing $AI_{DNAfrag}$ with $AI_{DNAcond}$ independently of the cell type (tumor cells or T-cells) and without considering the tumor entity in 81.6% of tissues an $AI_{DNAfrag} > AI_{DNAcond}$ was found (Fig.1). An opposite pattern ($AI_{DNAfrag} < AI_{DNAcond}$) was measured in 10.5% of the tissues examined. An equal number of apoptoses using both methods was detected in 2.6%.

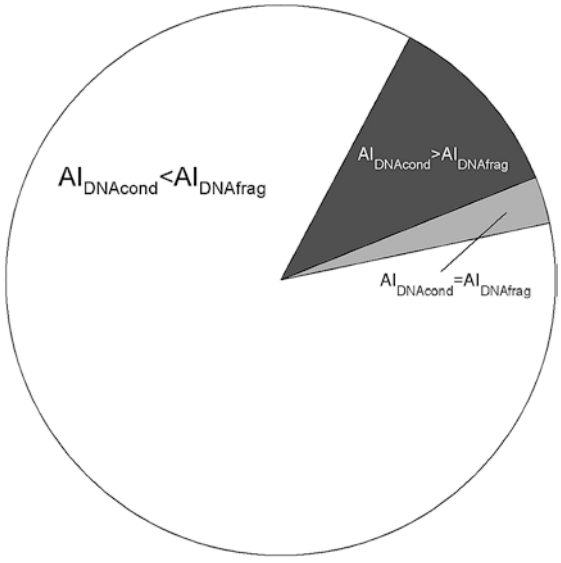

Fig. 1 The detection of apoptosis with two different methods leads to similar results in 2.6% of the examined tissues (n = 33). In most cases (81.6%), more cells with fragmented chromatin ($AI_{DNAfrag}$), as opposed to condensed chromatin ($AI_{DNAcond}$), were found. In certain cases (10.5%), the number of cells with condensed chromatin exceeded the number with fragmented chromatin. AIs could not be determined in 5.3% (data not shown)

Comparison of different AIs measured in both cell types with metastasis

Metastasized and non-metastasized tumors were pooled without considering the tumor entity (n = 33). From these 33 tissues the mean of the different AIs were calculated. T-cells as well as tumor cells of metastasized tumors showed a comparable distribution of different AIs (Fig. 2, *left panel*). A mean $AI_{DNAfrag}$ of 76 and 82% was found in T-cells and tumor cells, respectively. The mean $AI_{DNAcond}$ was 13 and 10% in T-cells and tumor cells, respectively. Both criteria for apoptosis detection were found in 11 and 8% (mean values) of T-cells and tumor cells, respectively.

In non-metastasized tumors a 10–20% lower $AI_{DNAfrag}$ was found in both cell types when compared with metastasized tumors. This was predominantly

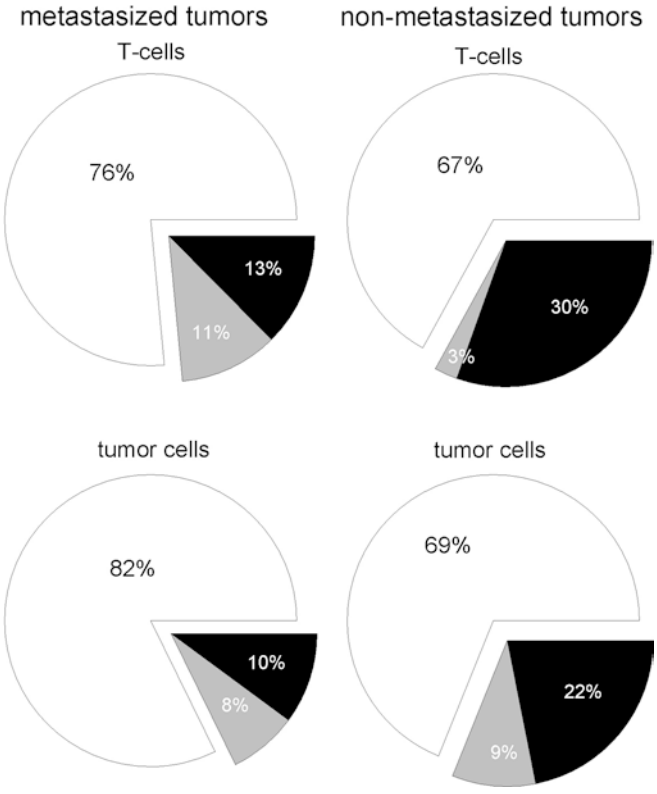

Fig. 2 Comparison of three different AIs (*white slices:* $AI_{DNAfrag}$, *black slices:* $AI_{DNAcond}$, *grey slices:* $AI_{DNAfrag\&cond}$) in metastasized and non-metastasized T-cells and tumor cells of 33 tissue samples. AIs represent mean values of the examined tissues

caused by an increased number of $AI_{DNAcond}$. The mean $AI_{DNAcond}$ was 30% in T-cells and 22% in tumor cells (Fig. 2, *right panel*).

Comparison of different AIs measured in both cell types and different tumor entities with metastasis

Metastasized embryonal cell carcinoma (n = 10) showed a mean $AI_{DNAfrag}$ of 88 and 93% in T-cells and tumor cells (Fig. 3, *left panel*), while a lower mean $AI_{DNAfrag}$ of 73 and 71% was found in T-cells and tumor cells of non-metastasized embryonal cell carcinoma (n = 6). Metastasized T-cells and tumor cells of mixed cell carcinoma (n = 8) revealed a mean $AI_{DNAfrag}$ of 82 and 80%. However, lower mean $AI_{DNAfrag}$ were found in non-metastasized (n = 9) T-cells (66%) and tumor cells (75%, Fig. 3, *right panel*). In other words, even when taking into account the tumor entity, a reduced mean number (about 10%) of $AI_{DNAfrag}$ were found in non-metastasized compared with metastasized tumors (Fig. 3). Again, this tendency appeared independently of the cell type. As shown before, these changes were mainly caused by an increased $AI_{DNAcond}$. Non-metastasized embryonal T-cells and tumor cells showed a mean $AI_{DNAcond}$ of 19% each, which contrasts with the mean $AI_{DNAcond}$ of 0.5 and 3% measured in metastasized embryonal T-cells and tumor cells. Likewise, T-cells and tumor cells of non-metastasized mixed cell carcinomas showed a mean $AI_{DNAcond}$ of 32 and 17%, while a mean $AI_{DNAcond}$ of 13 and 12% was measured in T-cells and tumor cells of metastasized mixed cell carcinomas.

Comparison of mean and SD of different AIs measured in both cell types with metastasis

The mean and SD of four different AIs ($AI_{DNAfrag}$, $AI_{DNAcond}$, $AI_{DNAfrag\&cond}$ and $AI_{totalapopt}$) measured in T-cells and tumor cells separately were compared with metastasis for the purpose of calculating statistically significant differences. In none of the cases was a significant difference calculated (p values typically ranged between 0.58 and 0.91, only AI 3 and AI7 revealed lower p values but not statistically significant differences [$p = 0.11$]) due to >100% interindividual differences in the AIs measured (Fig. 4). In detail, the mean of $AI_{DNAfrag}$ for metastasized T-cells (14.7% ±21.3) was higher compared with non-metastasized T-cells (10.9% ±17.5). The same was found for $AI_{totalapopt}$ (metastasized T-cells: 15.7% ±21.1 and non-metastasized

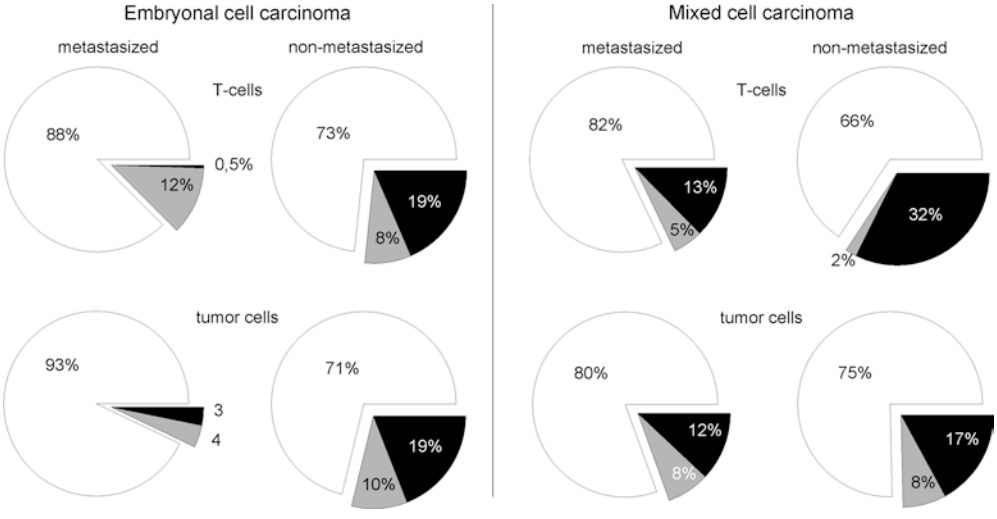

Fig. 3 Comparison of three different AIs (*white:* $AI_{DNAfrag}$, *black:* $AI_{DNAcond}$, *grey:* $AI_{DNAfrag\&cond}$) separately measured in metastasized and non-metastasized tissues of embryonal and mixed cell carcinoma origin. The percentages and slices represent the corresponding mean values of AIs of T-cells and tumor cells

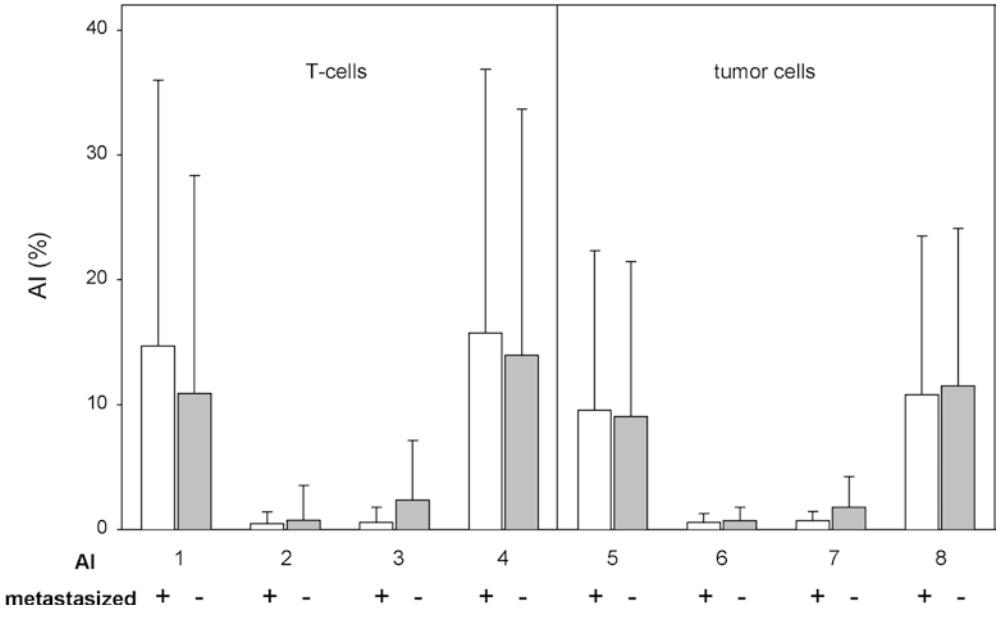

Fig. 4 Comparison of mean values and SD values of different AIs in T-cells (*1* $AI_{DNAfrag}$, *2* $AI_{DNAfrag\&cond}$, *3* $AI_{DNAcond}$, *4* $AI_{totalapopt}$) and tumor cells (*5* $AI_{DNAfrag}$, *6* $AI_{DNAfrag\&cond}$, *7* $AI_{DNAcond}$, *8* $AI_{totalapopt}$) of metastasized and non-metastasized tumors

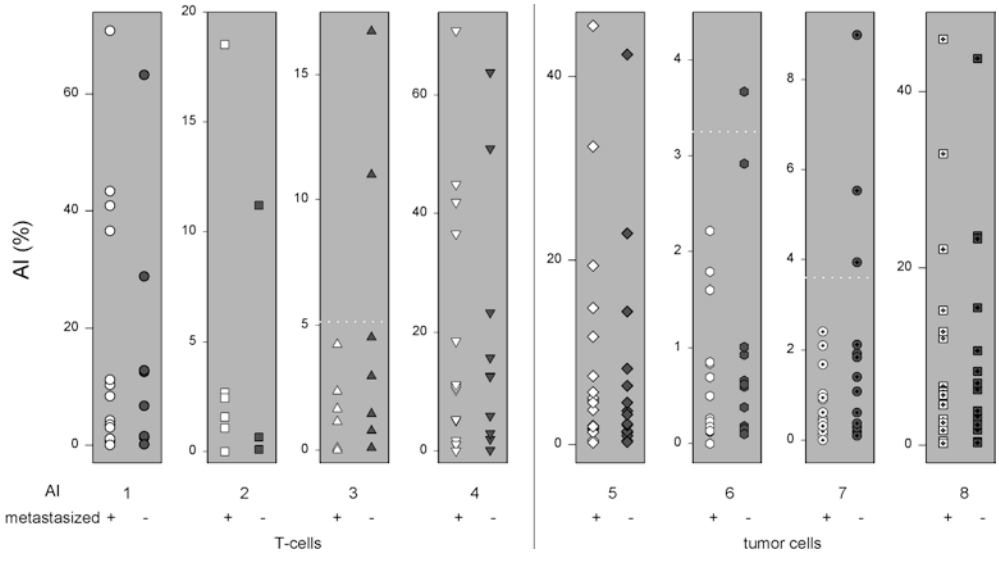

Fig. 5 Comparison of the distribution of the individual AIs of tumor tissues. The distribution of metastasized and non-metastasized AIs of T-cells (*1* $AI_{DNAfrag}$, *2* $AI_{DNAfrag\&cond}$, *3* $AI_{DNAcond}$, *4* $AI_{totalapopt}$) and tumor cells (*5* $AI_{DNAfrag}$, *6* $AI_{DNAfrag\&cond}$, *7* $AI_{DNAcond}$, *8* $AI_{totalapopt}$) was compared. The *horizontal dotted white line* indicates the interval up to which 99.99% (SD×4) of metastasized AI values were distributed. Non-metastasized AI values lying beyond that line were assumed to represent AI values lying outside the distribution of metastasized AIs

T-cells: 14.0% ±19.7). Comparable mean values for $AI_{DNAfrag\&cond}$ were found in metastasized and non-metastasized T-cells (0.5% ±0.9 versus 0.7% ±2.8). Decreased mean values of $AI_{DNAcond}$ were found in metastasized compared with non-metastasized T-cells (0.6% ±1.2 as opposed to 2.3% ±4.8).

Tumor cells revealed comparable results. However, the mean of $AI_{DNAfrag}$ for metastasized tumor cells (9.5% ±12.8) was comparable to non-metastasized tumor cells (9.0% ±12.4). The same could be found for $AI_{DNAfrag\&cond}$ (metastasized tumor cells: 0.6% ±0.7 and non-metastasized tumor cells: 0.7% ±1.1). Decreased mean values of $AI_{DNAcond}$ were found in metastasized compared with non-metastasized tumor cells (0.7% ±0.8 versus 1.8% ±2.5). The same was found for $AI_{totalapopt}$ (metastasized tumor cells: 10.8% ±12.7; non-metastasized tumor cells: 11.5% ±12.6).

Comparison of individual tumor AIs measured in both cell types with metastasis

Individual AIs, but not mean values, of T-cells and tumor cells measured in different tumors (tumor entity not considered) were compared with regard to metastasis (Fig. 5). This procedure made it possible to search for tumor values lying outside the assumed Gaussian distribution. The *horizontal dotted white line* indicates the interval up to which 99.99% (SD×4) of metastasized AI values were distributed. Non-metastasized AI values lying beyond that line were assumed to represent AI values lying outside the distribution of metastasized AIs. By and large, no differences in the individual AI distribution of metastasized and non-metastasized tumors could be found (T-cells: $AI_{DNAfrag}$, $AI_{DNAfrag\&cond}$ and $AI_{totalapopt}$; tumor cells: $AI_{DNAfrag}$ and $AI_{totalapopt}$).

However, in T-cells two non-metastasized tumors showed $AI_{DNAcond}$ (11.0 and 16.7%), which considerably exceeded the 99.99% interval of 5% (Fig. 5, AI 3). The same could be shown for one tumor in AI 6 (tumor AI: 3.7%, 99.99%-interval: 3.2%) and three tumors in AI 7 (tumor AI: 9.0%, 5.5% and 3.9%, 99.99% interval: 3.5%).

Furthermore, the height of AIs of T-cells relative to the corresponding AIs of tumor cells was correlated with metastasis, which produced ratios as shown in Fig. 6. Again, a *horizontal dotted dark grey line* was defined, which indicates the interval up to which 99.99% (SD×4) of non-metastasized AI ratios were distributed. AI ratios of metastasized tumors lying beyond that line were assumed to represent AI ratios lying outside the distribution of non-metastasized tumors. Only one AI ratio (AI ratio 3/7) showed a comparable distribution of individual AI ratios of metastasized and non-metastasized tumors. The other five AI ratios revealed increased AI ratios, but always and only for metastasized tumors (AI 1/5 tumor: 24.8%, 99.99% interval: 11.0%; AI 2/6 tumors: 5.5%, 37.3%, 99.99% interval: 3.7%; AI 4/8 tumor: 24.8%, 99.99% interval: 5.2%; AI[1 + 2]/[5 + 6] tumor: 20.5%, 99.99% interval: 10.2%; AI [2 + 3]/[6 + 7] tumor: 16.8%, 99.99% interval: 3.8%). The same analysis was repeated, but with the tumor entity being taken into account. The results are summarized in Table 3.

Table 3 List of tumors with AIs lying outside the 99.99% interval of metastasized or non-metastasized tumors. The second column gives the number of AIs per tumor which showed differences from the 99.99% interval. For instance, tumor 11 showed only one AI with a value lying outside the 99.99% interval, while tumor 9 showed differences lying over the 99.99% interval for three different AIs. The left side of the table shows tumors with AIs lying outside the 99.99% interval without consideration of the tumor entity, which, however, is taken into account on the right side of the table

Without consideration of tumor entity		Considering tumor entity:			
		EZ		MZ	
Tumor #	# AI	Tumor #	# AI	Tumor #	# AI
11	1	5	1	23	1
24	1	9	1	36	1
2	2	2	2	38	1
13	2	6	2	24	3
6	3	12	3	-	-
9	3	17	3	-	-

Without consideration of the tumor entity, six out of 33 tumors showed AI values and/or AI ratios lying outside the 99.99% interval for one, two or three AIs (for details see Table 3). When taking into account the tumor entity, as many as ten out of 33 tumors revealed AI values and/or AI ratios lying outside the 99.99% interval (summarized data shown in Table 3).

Fig. 6 The distribution of metastasized and non-metastasized ratios calculated from different AIs of T-cells with the corresponding AIs of tumor cells was compared. A h*orizontal dotted dark grey line* was defined, which indicates the interval up to which 99.99% (SD×4) of non-metastasized AI ratios were distributed. AI ratios of metastasized tumors lying beyond that line were assumed to represent AI ratios lying outside the distribution of non-metastasized tumors. Ratios of corresponding AIs from T-cells and tumor cells were calculated with the AIs defined as follows: T-cells (first number in parenthesis) and tumor cells (second number in parenthesis): *1/5* $AI_{DNAfrag}$, *2/6* $AI_{DNAfrag\&cond}$, *3/7* $AI_{DNAcond}$, *4/8* $AI_{totalapopt}$. In a few cases with AIs of 0%, these numbers were set at 0.1% (represents the average spontaneous apoptosis frequency measured in normal testis tissue) in order to calculate defined ratios

Discussion

Originally, apoptosis was defined on the basis of characteristic morphological features (e.g., DNA condensation along the nucleus membrane). Later, apoptosis became linked to certain processes of DNA cleavage. However, in vitro data suggested a discrepancy in the number of cells showing either apoptosis morphology or endonucleolytical DNA fragmentation [6, 17]. Only few in vivo data exist which deal with that question. Recently published data confirmed these earlier in vitro

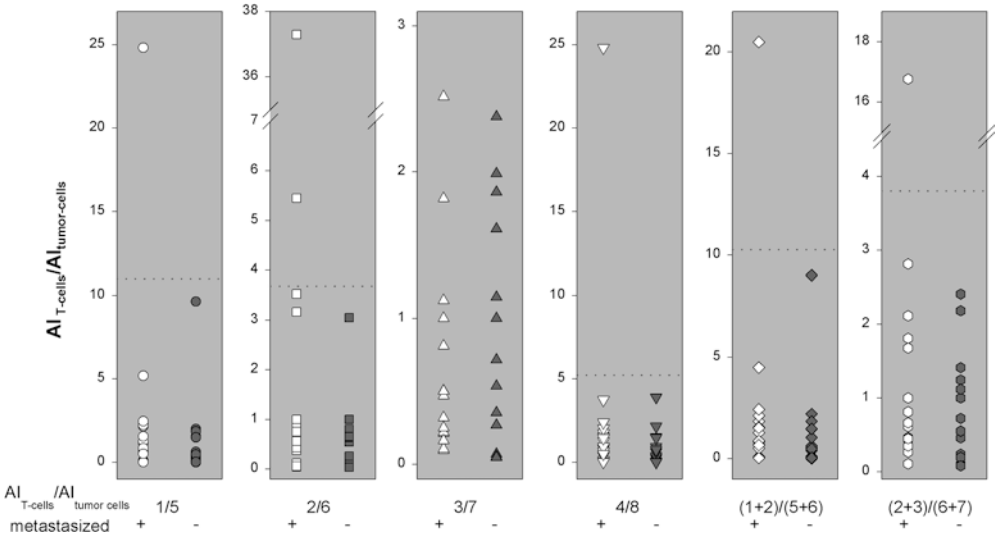

findings [1, 22]. The data shown here are in agreement with earlier findings, but examined on a different and larger cohort of tumors. Only a minority of testis tumors revealed comparable values of $AI_{DNAfrag}$ and $AI_{DNAcond}$ (2.6%, Fig. 1). Usually, $AI_{DNAfrag}$ exceeded the value of $AI_{DNAcond}$ (81.6%). But in 10.5% of the tissues examined, a reverse pattern evolved. These findings highlight the fact that measurements of apoptosis depend rather on the method used. These data help to explain the differences in the judgment of apoptosis significance for diagnostic, therapeutic and prognostic purposes [2, 9, 16, 24, 27, 7].

When examining the different AIs, it became evident that non-metastasized tumors revealed a lower number of $AI_{DNAfrag}$ ($\geq$ 10%) compared with metastasized tumors (Fig. 2). Interestingly, this difference was independent of the cell type and the tumor entity examined (Fig. 3). However, comparison of mean values of the AIs showed no significant differences with regard to the metastasis status (Fig. 4). This was attributable to large interindividual differences of the AIs calculated (Fig. 4). One could assume that these interindividual differences relate to tissue components of different origin in the mixed tumors. Nevertheless, the data shown above argue against that interpretation because the differences measured were independent of the cell type and the tumor entity measured. Moreover, when bearing in mind that AIs of tissue from one origin (embryonal cell carcinoma) reveal an interindividual difference which is comparable to that found in mixed tumors (data not shown), it is more likely that these differences refer to interindividual differences, but are less influenced by the tissue components of mixed tumors. This could be caused, for example, by bystander effects known to play an important role in the tumour response to ionizing radiation. Furthermore, our newest gene expression profiling data (submitted for publication) suggest that seminoma and non-seminoma from the gene expression point of view behave like ''mirror images,'' irrespective of the origin of the non-seminoma. This suggests that, from the genetic point of view, histological criteria are of minor importance. Since apoptosis is known to be regulated at the gene expression level, it is presumably more important to consider the individual data, as done in these examinations.

The discrepancy between the data shown above prompted us to examine the distribution of the AIs measured in each individual tissue (Figs. 5 and 6). Based on the AIs measured, their distribution in metastasized and non-metastasized tumors was compared and an interval which contains 99.99% (SD×4) of all values was calculated. Certain tumors showed AIs lying several times above this interval (for details, see Figs. 5 and 6). It is interesting to note that all these tumors revealed two characteristics: (1) non-metastasized tumor cells and T-cells showed higher AIs compared with metastasized tumors, and (2) All metastasized tumors of this group revealed 5 to 25-fold higher AIs of T-cells relative to the corresponding AIs of the tumor cells (Fig. 6). These characteristics were independent of the tumor entity and could be shown for six out of 33 tumors without considering the tumor entity. This number increased (ten out of 33 tumors) when taking into account the tumor entity (Table 3).

It is hypothesized that a selection in favor of the apoptosis-resistant phenotype takes place during tumorigenesis [4, 27, 21], which is shown in certain models [8, 10, 14, 18, 19, 25, 32]. Increased AIs [3, 28] or unchanged AIs [15] were found in a small number of models, thus supporting the hypothesis described above. Assuming that tumor progression to a metastatic state represents a further stage in tumorigenesis, the increased AIs found in a fraction of presumably less-developed non-metastasized tumor cells, as well as T-cells, could be explained.

Furthermore, we show here for the first time that metastasized tumors revealed a several-fold increase of AIs of T-cells compared with the corresponding AIs of the tumor cells. This could be interpreted as a successful counterattack of tumor cells, thus reducing the immunological attack of the organism but supporting the process of metastasis. The mechanism with which tumor cells counterattack lymphocytes has been investigated by different groups using different models. For instance, colon cancer cells could induce apoptosis in lymphocytes through the Fas system [33] and lymphocytes could induce apoptosis in cancer cells through the Fas system as well [5]. Although the Fas system appears of importance [25], especially in testis tumors, the absence of the Fas system's involvement in the counterattack of tumor cells and the attack through lymphocytes has been demonstrated [23]. An involvement of bax in apoptotic processes taking place in seminoma has been shown recently [34]. Whether this might explain our data has to be examined. Hence, the mechanism underlying our data presented here remains to be resolved.

Based on these findings, a tool for predicting metastasis could be developed. Table 3 depicts the number of AIs lying outside the 99.99% interval per individual tumor. For instance, seven tumors showed AIs lying outside the 99.99% interval for only one AI (Table 3). Depending on the robustness of the tool, the number of AIs lying outside the 99.99% interval per individual tumor has to be defined. In other words, five out of 33 tumors (15.2%) could be detected provided two or three AIs lying outside the 99.99% interval per tumor were considered (Table 3). Again, the majority of tumors characterized by a low apoptotic activity—probably due to development into an apoptosis-resistant phenotype—will not be detected by this method.

In summary, the AIs measured with different methods in vivo led in most cases to highly different results, which explains differences in the assessment of apoptosis significance for tumor prognosis. With regard to tumorigenesis, a fraction of non-metastasized testis tumors was characterized by higher AIs of tumor cells and T-cells compared with metastasized tumors, which could be interpreted as a characteristic of tumors in an earlier

stage of their development. We show here for the first time 5 to 25-fold higher AIs of T-cells relative to tumor cells of metastasized tumors, which suggests a successful counterattack of tumor cells, thus supporting the process of metastasis. However, only ten out of 33 tumors revealed these changes of AI, which again highlights the fact that tumor biology cannot be predicted by a single parametric approach. It remains to be shown whether these characteristics might be suitable for a reliable prediction of metastasis. Furthermore, it must be shown whether these measurements can be confirmed using a larger cohort of biopsies.

Acknowledgments We very much appreciate the accurate technical work of A. Pflüger. We also wish to stress our thanks to Mrs. B. Hay, Department of Biometry and Medical Documentation, University of Ulm, who contributed valuable recommendations from a biomathematical point of view. This work was supported by a special research grant from the German Ministry of Defense.

References

1. Abend M, Schmelz HU, Kraft K, Rhein AP, van Beuningen D, Sparwasser, C (1998) Inter-comparison of apoptosis morphology with active DNA cleavage on single cells in vitro and on testis tumours. J Pathol 185:419
2. Aftabuddin M, Yamadori I, Yoshino T, Kondo E, Akagi, T (1995) Correlation between the number of apoptotic cells and expression of the apoptosis-related antigens Fas, Leyand bcl-$_2$ protein in non-Hodgkins lymphomas. Pathol Int 45:422
3. Agui T, McConkey DJ, Tanigawa N (2002) Comparative study of various biological parameters, including expression of surviving, between primary and metastatic human colonic adenocarcinomas. Anticancer Res 22:1769
4. Brown JM, Wouters BG (1999) Does apoptosis contribute to tumor cell sensitivity to anticancer agents? In: Hickman JA, Dive C (eds) Apoptosis and cancer chemotherapy. Humana Press, Totowa, NJ, pp. 1–18
5. Chen YL, Wang JY, Chen SH, Yang BC (2002) Granulocytes mediates the Fas-L-associated apoptosis during lung metastasis of melanoma that determines the metastatic behaviour. Br J Cancer 87:359
6. Del Bino G, Darzynkiewicz Z, Degraef C, Mosselmans R, Fokan D, Galand P (1999) Comparison of methods based on annexin-V binding, DNA content or TUNEL for evaluating cell death in HL-60 and adherent MCF-7 cells. Cell Prolif 32:25
7. El-Ahmady O, El-Salahy E, Mahmoud M, Wahab MA, Eissa S, Khalifa A (2002) Multivariate analysis of bcl-2, apoptosis, P53 and HER-2/neu in breast cancer: a short-term follow-up. Anticancer Res 22:2493
8. Fernandez Y, Gu B, Martinez A, Torregrosa A, Sierra A (2002) Inhibition of apoptosis in human breast cancer cells: role in tumor progression to the metastatic state. Int J Cancer 101:317
9. Fisher, DE (1994) Apoptosis in cancer therapy: crossing the threshold. Cell 78:539
10. Izawa JI, Sweeney P, Perrotte P, Kedar D, Dong Z, Slaton JW, Karashima T, Inoue K, Benedict WF, Dinney CP (2002) Inhibition of tumorigenicity and metastasis of human bladder cancer growing in athymic mice by interferon-beta gene therapy results partially from various antiangiogenic effects including endothelial cell apoptosis. Clin Cancer Res 8:1258
11. Kerr JFR, Wyllie AH, Currie AR (1972) Apoptosis: a basis biological phenomenon with wide-ranging implications in tissue kinetics. Br J Cancer 26:239
12. Kradin RL, Bhan AK (1993) Tumor infiltrating lymphocytes. Lab Invest 69:635
13. Levine EL, Davidson SE, Roberts SA, Chadwick CA, Potten CS, West CML (1994) Apoptosis as predictor of response to radiotherapy in cervical carcinoma. Lancet 44:344
14. Li L, Yan L, Wei Y, Liu Z, Wang Z, Lei S, Huang G (1999) Significance of apoptosis status and apoptosis-associated antigen expression in human colorectal adenocarcinoma sequence. Hua Xi Yi Ke Da Xue Xue Bao 30:185
15. Lopez T, Hanahan D (2002) Elevated levels of IGF-1 receptor convey invasive and metastatic capability in a mouse model of pancreatic islet tumorigenesis. Cancer Cell 1:339
16. Lu QL, Elia G, Lucas S, Thomas JA (1999) Bcl-$_2$ proto-oncogene expression in Epstein-Barr-virus-associated nasopharyngeal carcinoma. Int J Cancer 53:29
17. Oberhammer F, Wilson JW, Dive C, Morris ID, Hickman JA, Wakeling AE, et al. (1993) Apoptotic death in epithelial cells: cleavage of DNA to 300 and/or 50 kb fragments prior to or in the absence of internucleosomal fragmentation. EMBO J 12:3679
18. Oliver L, Cordel S, Barbieux I, LeCabellec MT, Meflah K, Gregoire M, Vallette FM (2002) Resistance to apoptosis is increased during metastatic dissemination of colon cancer. Clin Exp Metast 19:175
19. Richter EN, Oevermann K, Buentig N, Storkel S, Dallmann I, Atzpodien J (2002) Primary apoptosis as a prognostic index for the classification of metastatic renal cell carcinoma. J Urol 168:460
20. Rupnow BA, Knox SJ (1999) The role of radiation-induced apoptosis as a determinant of tumor responses to radiation therapy. Apoptosis 4:115
21. Scaife CL, Kuang J, Wills JC, Trowbridge DB, Gray P, Manning BM, Eichwald EJ, Daynes RA, Kuwada SK (2002) Nuclear factor kappaB inhibitors induce adhesion-dependent colon cancer apoptosis: implications for metastasis. Cancer Res 62:6870
22. Schmelz HU, Abend M, Kraft K, van Beuningen D, Pust R, Sparwasser C (1999) Apoptosis in human embryonal cell carcinoma; preliminary results. Urol Res 27:368
23. Schmelz HU, Abend M, Kraft K, Hauck EW, Weidner W, van Beuningen D, Sparwasser, C (2002) Fas/Fas ligand system and apoptosis induction in testicular carcinoma. Cancer 95:73
24. Schmitt CA, Lowe SW (1999) Apoptosis and therapy. J Pathol 187:127
25. Shin MS, Kim HS, Lee SH, Lee JW, Song YH, Kim YS, Park WS, Kim SY, Lee SN, Park JY, Lee JH, Xiao W, Jo KH, Wang YP, Lee KY, Park YG, Kim SH, Lee JY, Yoo NJ (2002) Alterations of Fas-pathway genes associated with nodal metastasis in non-small cell lung cancer. Oncogene 21:4129
26. Staunton MJ, Gaffney EF (1995) Tumor type is a determinant of susceptibility to apoptosis. Am J Clin Pathol 103:300
27. Steel G (2001) The case against apoptosis (review article). Acta Oncol 40:968
28. Termuhlen PM, Sweeney-Gotsch BM, Berman RS, Ellis LM, Bucana C, Shen Y, Cleary KR, McConkey DJ (2002) Increased apoptosis in metastatic human colonic adenocarcinomas Cancer Biol Ther 1:58
29. Walker PR, Sikorska M (1997) New aspects of the mechanism of DNA fragmentation in apoptosis. Biochem Cell Biol 75:287
30. Walker PR, Pandey S, Sikorska M (1995) Degradation of chromatin in apoptotic cells. Cell Death Diff 2:97
31. Wheeler JA, Stephens LC, Tornos C, et al (1995) ASTRO research fellowship: apoptosis as a predictor of tumor response to radiation in stage IB cervival carcinoma. Int J Rad Oncol Biol Phys 32:1487
32. Yamamoto T, Oda K, Kubota T, Miyazaki K, Takenouti Y, Nimura Y, Hamaguchi M, Matsuda S (2002) Expression of p73 gene, cell proliferation and apoptosis in breast cancer: Immunohistochemical and clinicopathological study. Oncol Rep 9:729
33. Zhu Q, Deng C (2002) Apoptosis of lymphocytes induced by Fas/FasL of colon cancer cells. Ai Zheng 21:272
34. Grobholz R, Zentgraf H, Kohrmann KU, Bleyl U (2002) Bax, Bcl-2, fas and Fas-L antigen expression in human seminoma: correlation with the apoptotic index. APMIS 110:724